coatings

MDPI

Review

Functional Coatings for Fiber Bragg Gratings: A Critical Review of Deposition Techniques for Embedded and Harsh-Environment Applications

Cristian Vendittozzi [1,*], Emilia Di Micco [1], Michele A. Caponero [2] and Rosaria D'Amato [2]

[1] Department of Chemical Engineering Materials Environment, Sapienza University of Rome, Via Eudossiana 18, 00184 Roma, Italy; emilia.dimicco@uniroma1.it
[2] ENEA Centro Ricerche Frascati, Via Enrico Fermi 45, 00044 Frascati, Italy; michele.caponero@enea.it (M.A.C.); rosaria.damato@enea.it (R.D.)
* Correspondence: cristian.vendittozzi@uniroma1.it

Abstract

Fiber Bragg Grating (FBG) sensors facilitate compact, multiplexed, and electromagnetic interference-immune monitoring in embedded and harsh environments. The removal of the polymer jacket, a measure taken to withstand elevated temperatures or facilitate integration, exposes the fragile glass. This underscores the necessity of functional coatings, which are critical for enhancing durability, calibrating sensitivity, and improving compatibility with host materials. This review methodically compares coating materials and deposition routes for FBGs, encompassing a range of techniques including top-down physical-vapor deposition (sputtering, thermal/e-beam evaporation, cathodic arc), bottom-up chemical vapor deposition (CVD)/atomic layer deposition (ALD), wet-chemical methods (sensitization/activation, electroless plating (EL), electrodeposition (ED)), fusion-based processes (casting and melt coating), and hybrid stacks (e.g., physical vapor deposition (PVD) seed → electrodeposition; gradient interlayers). The consolidation of surface-preparation best practices and quantitative trends reveals a comprehensive understanding of the interrelationships between coating material/stack, thickness/microstructure, adhesion, and sensitivity across a range of temperatures, extending from approximately 300 K to cryogenic regimes. Practical process windows and design rules are distilled to guide method selection and reliable operation across cryogenic and high-temperature regimes.

Keywords: fiber Bragg grating (FBG); metallic coating; sputtering; electroless plating; electrodeposition; cryogenic sensing; high-temperature sensing; embedded sensors

Academic Editors: Tsvetanka Babeva, Gergana Alexieva and Rositsa Gergova

Received: 22 September 2025
Revised: 18 October 2025
Accepted: 20 October 2025
Published: 2 November 2025

Citation: Vendittozzi, C.; Di Micco, E.; Caponero, M.A.; D'Amato, R. Functional Coatings for Fiber Bragg Gratings: A Critical Review of Deposition Techniques for Embedded and Harsh-Environment Applications. *Coatings* **2025**, *15*, 1268. https://doi.org/10.3390/coatings15111268

1. Introduction

Optical fiber Bragg grating (FBG) sensors are compact, multiplexable, immune to electromagnetic interference, and compatible with long-distance interrogation. These qualities have enabled the adoption of FBG sensors in biomedical monitoring, structural health monitoring, and industrial automation [1–4]. Beyond reviews specific to FBGs, comprehensive surveys of fiber-optic chemical and physical sensors, as well as distributed/networked sensing, provide a broader landscape for scalability and deployment [5–7]. In harsh or unconventional environments, such as cryogenic or high-temperature environments, radiation environments, environments with strong magnetic fields, or environments with vibration, bare gratings and standard packaging have limitations. This motivates the development of coatings and tailored processes that stabilize the optical response and extend

operability [8,9]. Recent overviews focusing on cryogenic FBG temperature sensing further emphasize the importance of coating-based designs at lower temperatures [10].

Despite their versatility, bare FBGs face inherent limitations when exposed to demanding operational environments. Silica core and cladding are brittle and prone to microcracking under thermal shock or strain concentration, and the polymer jacket, typically used for protection, softens or degrades above ~150 °C [11]. At cryogenic temperatures, the low thermo-optic coefficient of silica reduces temperature sensitivity and complicates calibration, while repeated cool-down cycles induce mechanical fatigue at the grating–coating interface [12]. In aerospace applications, sensors must endure vibration, low pressure, and wide thermal excursions, while maintaining adhesion and spectral integrity under cyclic mechanical loading [13]. In energy systems, including fusion and high-temperature components, FBGs experience intense gradients and radiation that can induce refractive index drift and signal degradation [12,14]. Similarly, in structural and civil infrastructures, long-term performance requires mechanical robustness and environmental stability over millions of strain cycles [15]. Across these sectors, industries demand FBGs that maintain linearity, adhesion, and repeatability from cryogenic to ultra-high temperatures, often when embedded within metal or composite hosts. These requirements have driven the integration of functional coatings—metallic, ceramic, or hybrid—to extend FBG operability beyond the range of bare gratings and ensure compatibility with advanced structural materials [12–15]. Alternatively, FBGs can also be inscribed through polymer coatings using ultraviolet (UV) radiation; however, such gratings often suffer from poor inscription uniformity, mechanical instability, and limited thermal endurance, restricting their applicability in harsh or high-temperature environments [16–18].

Although baseline demonstrations established FBG thermometry from ~2–400 K with appropriate packaging, sensitivity and stability degrade toward the deepest cryogenic conditions without additional engineering of the grating–host interface [19,20]. Early design studies of cryogenic FBG thermometers and femtosecond (fs)-inscribed gratings highlight inscription and packaging choices that affect the coating's response at low temperatures [21,22]. Representative applications include aeronautical structural health monitoring [23], conceptual designs for cryogenic and energy systems [24], and fusion-relevant strain monitoring on tungsten divertors [25]. Each application imposes constraints on geometry, survivability, and electromagnetic compatibility that coatings can help relieve. These constraints can be addressed by adding mechanical protection, improving thermal/mechanical coupling, providing hermetic barriers, and enabling bonding to metals or ceramics, all of which can be achieved through coatings. Polymeric layers (e.g., polymethyl methacrylate, PMMA) boost apparent temperature sensitivity and ease cycling, while metallic coatings (e.g., Ni, Cu, Zn, and Sn, as well as their combinations) offer higher thermal conductivity and robust attachment. Ceramic/oxide overlayers (e.g., TiN, TiO_2, and ZnO) cap against oxidation and interrupt diffusion [26–30]. Multilayer and duplex designs, such as Ni/Cu/Au or Ni/Zn, are often used to balance adhesion, diffusion control, and thermo-mechanical performance across a wide temperature range [28–31]. Gradient metallic coatings, which are specifically designed for cryogenic sensitivity and cyclic stability, broaden this design space and offer an alternative to simple duplex builds [32]. Nanostructured coating approaches and comparative analyses of thermal-sensing performance further expand the design space and clarify the trade-offs between sensitivity and transient response [33,34]. A variety of deposition routes are available. Top-down physical vapor deposition (PVD), including magnetron/ion beam sputtering (IBS) and thermal/e-beam evaporation, delivers controlled thin films. Bottom-up chemical vapor deposition (CVD)/atomic layer deposition (ALD) provides conformal oxides. Wet-chemical workflows, such as sensitization/activation and electroless (EL)/electrodeposition (ED), en-

able uniform metal builds and thick overcoats at low thermal budgets. Fusion-based routes, such as casting, integrate FBGs into metallic hosts. Hybrid flows, such as PVD seeding followed by ED or graded interlayers, combine the advantages of multiple routes [35].

General primers on thin films and processes complement this taxonomy by highlighting stress and roughness control on cylindrical substrates [36]. Practical metallization and re-coating procedures tailored to fibers are discussed in more detail later in the manuscript, and additional methods are cataloged in foundational surveys [37]. These methods have key engineering constraints. Strong adhesion to silica usually necessitates surface preparation and seed layers (e.g., $SnCl_2/PdCl_2$ activation for EL Ni-P). Residual stress and thickness-induced cracking impose limitations, especially for EL deposits, when the process window is exceeded [38,39]. At elevated temperatures, interdiffusion (e.g., Cu/Ni) and hydrogen uptake during plating can degrade coatings and spectra, unless barrier layers and post-bakes are employed [40]. At cryogenic temperatures, metallic overcoats increase thermal mass and can slow step response—a trade-off that must be balanced against sensitivity gains [41]. These considerations motivate the structured comparison and synthesis that follow.

1.1. Review Scope and Method

This review centers on coated FBGs operating from cryogenic to high-temperature regimes. Sources were identified in major databases (Scopus, Web of Science, IEEE Xplore, SPIE) using combinations of FBG with coating/metallization and process terms (PVD, ALD/CVD, EL, ED, casting) and environmental terms (cryogenic, high temperature, harsh environment). Publications from 2000 to 2025 were considered, with earlier seminal works included that were historically informative. Studies were retained when reporting coating material/stack, process details, thickness, temperature window, and sensitivity or durability metrics; purely numerical papers were used selectively to frame design rules (e.g., optimal thickness vs. temperature) [38,42]. Emphasis is placed on metallic and hybrid stacks, with polymers and oxides treated as contrasts or barriers where relevant [25,30]. Method taxonomy follows standard coating overviews to ensure consistent terminology [43,44], and general process primers offer additional context [36,37].

Figure 1 schematically maps the relationships among application domains, coating materials, and deposition routes, highlighting how environmental requirements guide both stack design and process selection. The comparative data for each regime are summarized in Table 1. Figure 2 introduces the stack archetypes referenced throughout the paper.

Table 1. Environmental drivers and representative coating strategies for fiber Bragg gratings. Arrow widths in Figure 1 qualitatively represent the frequency of the same combinations in the literature. The same acronyms presented in Figure 1 are used.

Environment	Dominant Degradation Drivers	Recommended Coating Stack	Deposition Route	Key Parameters/Post-Treatments	Normalized Sensitivity η_T (×Bare) *	Trade-Offs/Notes	Refs.
Cryogenic (2–80 K)	Low thermo-optic slope of silica, thermal shock, brittleness	Ni → Zn duplex/Ni/Sn multilayer/Ni–P + Sn	EL Ni–P → ED Zn/Sn (or alternating Ni/Sn plating)	5–30 µm total; anneal 250 °C; H_2 bake	1.5–5×	Highest η^T gain; moderate transient penalty (~2× slower step); stress-balancing needed in multilayers	[27,29,38,41]

Table 1. *Cont.*

Environment	Dominant Degradation Drivers	Recommended Coating Stack	Deposition Route	Key Parameters/Post-Treatments	Normalized Sensitivity η_T (×Bare) *	Trade-Offs/Notes	Refs.
High-temperature (600–1000 °C)	Oxidation, interdiffusion, drift	Ni/Cu/Au multilayer ± TiN/Al_2O_3 cap	PVD seed → ED Ni/Cu → PVD Au (+CVD/ALD cap)	~1–10 µm each; H_2 bake before use	≈1× (stable slope)	Excellent stability to 1000 °C; diffusion control via multilayers	[30,31,40]
Radiation/ nuclear	Embrittlement, hydrogen accumulation, adhesion loss	Thick Ni	Evap seed → ED Ni	≥10 µm; post-plating bake mandatory	≈1×	Robust, but prone to H_2 blisters if unbaked	[45]
Embedded/ CTE-matched	Thermal-shock delamination, CTE mismatch	Graded Mo–Cu → Ni	Sputtered gradient → ED Ni	–	1–2×	Stress-relieved interface; process complex	[46,47]
Corrosive/ chemical	Bath attack, oxidation in service	Ni–P or Ni–P + Zn	EL Ni–P or EL → ED	–	1–2×	Low-cost route; limited cryo-stability	[48,49]

* $\eta^T = S_T^{coat} / S_T^{bare}$ is the normalized temperature sensitivity.

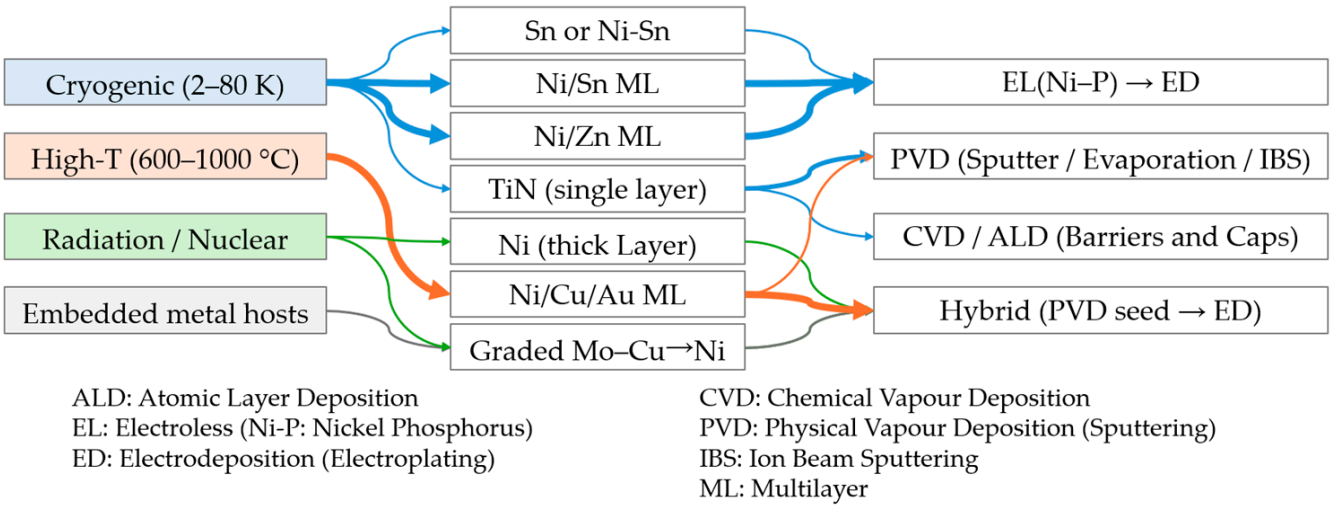

Figure 1. Landscape of coating-enabled fiber Bragg grating (FBG) sensing. Schematic diagram linking application domains (**left**), representative coating materials or multilayer stacks (**center**), and preferred deposition routes (**right**). Arrow thickness qualitatively represents the frequency of reported combinations in the literature. Color coding can follow temperature domain (light blue—cryogenic, orange—high-temperature, green—radiation, gray—embedded). The flow highlights how environmental requirements dictate both the choice of coating material and the deposition sequence.

1.2. Position of This Review Within Existing Literature

Several recent surveys address FBG technologies from application or instrumentation standpoints [5–9,20,21]. However, no studies have consolidated coating material, process and environment relationships into unified design rules. This review focuses on coatings as a design lever, standardizes key definitions (η_T, plateau thickness, transient penalty), and integrates surface prep, deposition, and post-treatment into clear selection criteria (Tables 1–8).

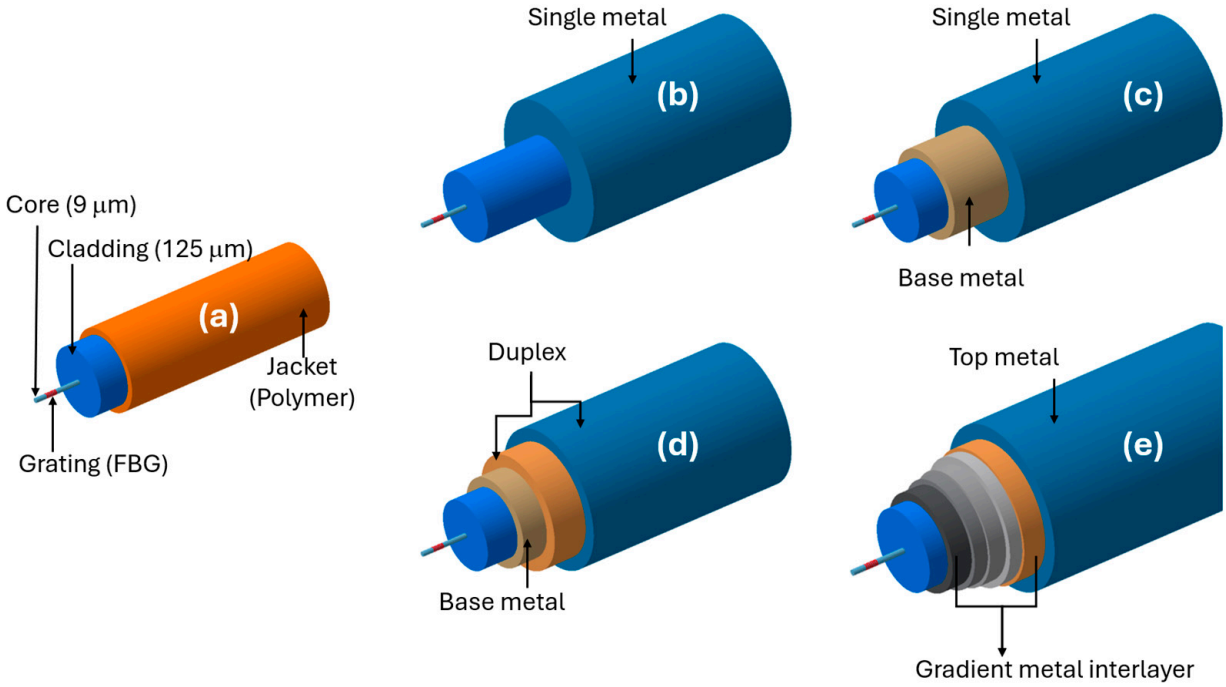

Figure 2. Schematic of coating-stack archetypes for FBGs: (**a**) standard 9/125 (core/cladding) fiber coated with a primary polymeric jacket; (**b**) single-layer metallic coating (e.g., Ni) providing direct thermo-mechanical coupling; (**c**) multilayer stack with a diffusion barrier (e.g., Ni/Cu/Au) designed to improve oxidation resistance and thermal durability; (**d**) duplex configuration (e.g., Ni/Cu or Ni → Zn) combining an adhesion layer with a high-CTE over-layer to enhance low-temperature sensitivity; and (**e**) graded interlayer (e.g., Mo–Cu) engineered to relieve residual stress between the fiber and the top metal. Single-layer and duplex coatings are typically used for cryogenic applications requiring strong strain transfer [27–29]; multilayers are employed for high-temperature or oxidizing environments [38,50]; and graded stacks are adopted for stress-relief and fatigue-resistant systems [51]. Common challenges across these architectures include interfacial delamination, residual stress accumulation, and spectral broadening with increasing coating thickness.

Table 2. Key Performance Parameters. Values are indicative ranges consolidated from [22,24,33,37,40,41,52].

Parameter	Symbol/Expression	Physical Meaning	Typical Range or Trend
Temperature sensitivity	$S_T = \frac{d\lambda_B}{dT}$	Apparent shift in wavelength per unit temperature	8–12 pm K^{-1} (bare), 12–50 pm K^{-1} (coated)
Normalized sensitivity	$\eta_T = \frac{S_T^{coat}}{S_T^{bare}}$	Sensitivity amplification due to coating	1–5 depending on material
Strain transfer efficiency	$\frac{\Delta\lambda_{strain,coat}}{\Delta\lambda_{strain,bare}}$	Degree of strain coupling between coating and fiber	0.5–1
Hysteresis	Δλ (heating vs. cooling)	Indicates elastic recovery and adhesion stability	<10 pm preferred
Drift	Δλ per cycle or time	Measures long-term thermal stability	<1 pm $cycle^{-1}$ typical
FWHM	Spectral width at ½ max	Indicates spectral broadening from strain gradients	0.1–0.3 nm typical
SNR	Peak reflectivity/noise	Evaluates spectral quality	>20 dB desirable
Response time	Time to 95% of Δλ after ΔT	Measures coating thermal inertia	0.1–5 s depending on thickness

Table 3. Surface preparation and activation workflow (parameters and controls).

Stage	Params	QA	Notes	Refs
Clean/etch	Solvent clean; acid/alkali etch	No residue; microscope	Avoid over-etching	[38,48]
Sensitize/activate	$SnCl_2 \rightarrow PdCl_2$	pH/time control	Foundation for EL nucleation	[48]
EL Ni–P seed	~90 °C; pH 4.5–5.0	Continuity; spectral check	Anneal removes λ(T) hysteresis	[38,53]
Electroplate build	Ni/Cu/Zn/Sn plating	Thickness per step; centroid drift	Bake Ni to outgas H_2	[39,40,51]
Barriers/caps	Thin TiN/oxides or Au	Adhesion; diffusion tests	Needed for Cu/Ni stacks	[30,54,55]
Post-treatments	Ni–P anneal; H_2 bake	Hysteresis removed; drift stabilized	Mandatory before qualification	[38,56]

Table 4. Quick plating parameter reference for common metals.

Metal	Bath	Current	Temp	Agitation	Notes	Refs
Ni	Watts/sulfamate	1–5 A/dm^2	45–60 °C	Moderate	H_2 uptake → bake	[40,51]
Cu	Acid sulfate	1–4 A/dm^2	20–30 °C	Moderate	Needs barriers/caps	[30,51]
Zn	Acid chloride/alkaline	0.5–2 A/dm^2	20–35 °C	Gentle	Recipe discipline for λ_0	[29,57,58]
Sn	Methanesulfonate/stannous	0.4–0.6 A/dm^2	20–30 °C	Gentle	Whisker mitigation	[51]

Table 5. Comparative synthesis of deposition routes.

Route	Thick	Conform	Stress	Rate	Complex	Defects	Best	Refs
PVD	0.01–2 µm	Good (LOS)	Low–Med	Low–Med	Med–High	Particles, stress	Seeds, TiN, thin Cu	[45,59,60]
CVD/ALD	0.005–0.2 µm	Excellent	Low	Low	High	Complex precursors	Barriers/caps	[54,55,61]
EL (Ni-P)	0.05–1 µm	Excellent	Med (anneal)	Med	Low	Nodules if bath aged	Uniform seeds	[40,62]
ED (Ni/Cu/Zn/Sn)	1–100 µm	Excellent (rotation)	Process-dependent	High	Low–Med	H_2, non-uniformity	Thick builds, duplex	[41,51]
Hybrid (PVD → ED)	0.1–50 µm	Good–Excellent	Balanced	Med–High	Med–High	Interface issues	Ni/Cu/Au multilayers	[30,31,63]
Graded interlayer	~1–10 µm	Good	Reduced	Med	High	Process complexity	Stress relief/embedding	[46]

To enable systematic comparison across the studies surveyed, Table 2 consolidates the key performance metrics commonly reported for coated FBG sensors. These parameters—spanning temperature sensitivity, hysteresis, drift, spectral quality, and transient response—form the quantitative framework adopted throughout this review. The same metrics are later used in Sections 3–6 to interpret coating material and process influences on performance.

Table 6. Recommended stacks and process windows by operating regime.

Regime	Stack	Depo	Treat	Caps	Notes	Refs
Deep cryo (≤80 K)	Ni → Zn duplex	Sn → Pd → EL Ni-P → Zn ED	Ni-P anneal; H_2 bake	—	Large slope, slower transient	[27,29,41,62]
80–300 K	Ni/Cu duplex or TiN	PVD seed → Ni/Cu ED	H_2 bake	TiN or Au	Balanced properties	[59,63,64]
High-T (600–1000 °C)	Ni/Cu/Au multilayer	PVD seed → ED → PVD cap	H_2 bake	Ni barrier + Au cap	Diffusion/oxidation control	[30,31,40]
Radiation/nuclear	Thick Ni	Evap Cr/Au → Ni ED	H_2 bake	—	Adhesion robustness	[45]
Embedded in metal host	Graded Mo–Cu → Ni	Sputter gradient → Ni ED	Stress-relief soaks	As needed	Shock survival	[46,64]

Table 7. Reporting template for reproducibility (per-specimen log).

Field	Desc	Refs
Specimen ID	ID, grating type	Example: FBG-01
Pre-coat spectral	λ_0, FWHM, SNR	1549.876 nm, 0.18 nm, 28 dB
Surface prep	Clean/etch details	Acetone/IPA, HF 0.5%
Activation/seed	$SnCl_2$ → $PdCl_2$; EL Ni-P	90 °C, pH 4.8, 0.15 µm
ED	Metal, current, thickness	Zn 0.6 A/dm^2, 8 min, +3 µm
Barriers/caps	Material, thickness	Au 80 nm PVD
Post-treatments	Anneal, bake	300 °C 60 min
Qualification	LN_2 cycles; soaks	5× 293↔77 K
Result summary	Slope, hysteresis	+2.3× bare
Failure mode	Adhesion, cracking	None after 10 cycles

The parameters listed in Table 2 establish the quantitative basis for evaluating the impact of coating material and deposition process. Temperature sensitivity (S_T) and its normalized form (η_T) quantify the thermo-mechanical coupling efficiency, while hysteresis and drift capture the stability of the coating–fiber interface under cyclic loading. Full width at half maximum (FWHM) and Signal-to-noise ratio (SNR) describe the spectral quality of the reflected signal, and response time reflects the thermal inertia introduced by the coating. Together, these metrics enable direct comparison across studies that differ in coating composition, geometry, and fabrication route.

In parallel with coating strategies, polarization-maintaining fibers—particularly PANDA (Polarization-maintaining AND Absorption-reducing fiber) designs—are being explored for low-temperature and harsh-environment sensing to mitigate birefringence-related drift and enhance readout stability, including recent cryogenic demonstrations using PANDA-PMF Sagnac architectures and high-temperature PANDA-based sensors [65,66].

Table 8. Classification of coatings and recommended use for FBG sensors.

Coating Type	Representative Materials	Typical Application Range	Main Advantages	Main Limitations	Typical Temperature Sensitivity/Accuracy *
Metallic (single-layer)	Ni, Cu, Al	Cryogenic (2–300 K), moderate thermal cycling	Strong strain transfer, easy deposition	Residual stress, oxidation	$\eta_T \approx 1.5$–3; ±0.5 K stability
Duplex/multilayer	Ni → Zn, Ni/Cu/Au, Ni/Sn	Cryogenic to 800 °C	Enhanced adhesion, tunable sensitivity	Complexity, interdiffusion	$\eta_T \approx 2$–5; ±0.3 K typical
Ceramic/oxide	TiO_2, SiO_2, Al_2O_3	600–1000 °C (oxidizing atmospheres)	High-T stability, oxidation resistance	Brittle, limited strain transfer	$\eta_T \approx 1$–1.5; ±1 K typical
Composite/ hybrid	Metal + polymer, Metal + oxide	100–500 °C, humidity/corrosion protection	Mechanical resilience, environmental sealing	Aging of polymer layers	$\eta_T \approx 1.2$–2; ±0.5 K
Polymeric/UV-resin	Acrylate, polyimide	<150 °C, low-cost use	Flexible, easy handling	Thermal degradation, poor uniformity	$\eta_T \approx 1$; ±1–2 K

* Indicative ranges consolidated from [22,24,33,37,40,41,50,52].

2. Fundamentals and Performance Metrics for Coated FBGs

Temperature sensing with fiber Bragg gratings (FBGs) relies on the shift in the Bragg wavelength as the effective refractive index and grating period vary with temperature. For a bare grating, the Bragg condition is given by the following:

$$\lambda_B = 2n_{eff}\Lambda \quad (1)$$

where n_{eff} is the effective refractive index of the fiber core and Λ is the grating period. The wavelength–temperature response of an uncoated silica grating can be expressed as follows:

$$S_T^{bare} = \frac{d\lambda_B}{dT} = \lambda_B\left(\alpha_{SiO_2} + \xi_{SiO_2}\right) \quad (2)$$

where α_{SiO_2} and $\xi_{SiO_2} = (1/n_{eff})(dn_{eff}/dT)$ are the thermal-expansion and thermo-optic coefficients of fused silica, respectively. This intrinsic slope typically lies around 8–12 pm K^{-1} near room temperature and decreases toward cryogenic conditions [2–4].

2.1. Thermo-Mechanical Coupling Induced by Coatings

When a grating is metalized, the coating imposes an additional axial strain through thermo-mechanical coupling. The apparent temperature sensitivity then reflects not only the intrinsic silica response but also the coefficient of thermal expansion (CTE) mismatch, elastic modulus, thickness, and adhesion quality of the over-layer. The effective slope can be described as follows:

$$S_T^{coat} = S_T^{bare} + \lambda_B\kappa(T,\ E_i,\ \alpha_i,\ t_i,\ adesion) \quad (3)$$

where E_i, α_i, and t_i denote, respectively, Young's modulus, Coefficient of Thermal Expansion (CTE), and thickness of the i-th layer, and κ is a strain-transfer function that captures mechanical coupling between the coating and the fiber core. As coating thickness increases, a greater fraction of the thermal load is transferred to the metal, and the apparent slope increases monotonically until a plateau is reached. Beyond this point, additional build yields diminishing returns while increasing residual stress, roughness, and cracking [38,42,67,68]. The height and position of the plateau depend on the metal's CTE, modulus, and interface quality. Softer and higher-CTE metals such as Zn or Sn provide large low-temperature gains at moderate thickness, whereas stiffer metals such as Ni require thicker deposits to approach the plateau but offer better adhesion and high-temperature stability [32,38,67]. Duplex and multilayer stacks exploit these contrasts, allocating thickness among layers to maximize sensitivity while avoiding localized stress.

The archetypes of coating architectures used throughout this review are illustrated in Figure 2, which distinguishes single-layer, duplex, multilayer, and graded interlayer configurations [27–29,38,50,51].

2.2. Normalized Temperature Sensitivity and Key Metrics

Because reported slopes vary across studies, normalized quantities are used for consistent comparison. The normalized temperature sensitivity is defined as follows:

$$\eta_T = S_T^{coat} / S_T^{bare} \tag{4}$$

This was evaluated for the same temperature range. Values of $\eta_T > 1$ denote amplification of the Bragg response due to coating; $\eta_T < 1$ indicates attenuation caused by stiff or poorly bonded films. Reported η_T values typically fall between 1.5 and 5 for cryogenic metallic coatings such as Ni → Zn duplex or Ni/Sn multilayers [27,29,38], whereas high-temperature multilayers (Ni/Cu/Au) maintain $\eta_T \approx 1$ but provide long-term stability. To evaluate coating integrity and spectral quality, the following metrics are consistently used [38]:

- Spectral centroid shift (for mean λ stability);
- FWHM (for spectral broadening);
- SNR (for reflectivity quality);
- Hysteresis between heating/cooling;
- Drift per thermal cycle;
- Response time to step changes in temperature.

Stable coatings preserve a narrow, high-SNR reflection with minimal centroid drift after each growth step or anneal.

The architecture illustrated in Figure 2 summarizes the evolution of coating design for FBGs. Single-layer coatings (typically Ni, Cu, or Al) are used when simple mechanical reinforcement and moderate sensitivity enhancement are sufficient. Duplex coatings introduce a seeding or adhesion layer beneath a high-CTE top layer to boost low-temperature response while maintaining fiber adhesion. Multilayer and graded coatings are developed to distribute thermal stress and prevent cracking during cyclic heating or cooling, making them suitable for high-temperature aerospace or power applications. Hybrid or composite coatings, which may include metallic, oxide, or polymeric sublayers, offer environmental sealing and compatibility with composite host materials. Each configuration represents a compromise between strain transfer efficiency, residual stress control, and environmental resistance.

2.3. Reporting Conventions and Comparison Framework

This review interprets the literature using consistently defined metrics and test profiles so that disparate studies can be compared on common ground [2–4]. Spectral and thermal responses are reported at standardized processing checkpoints: before coating, after seeding, after each build increment, and after post-treatments. Coating stacks are written from the glass outward, with layer thicknesses where specified; deposition routes are identified per layer (e.g., PVD seed → EL Ni–P → electroplated Ni; sputtered TiN single-layer; duplex Ni → Zn with EL seed), and post-treatments are stated explicitly (e.g., short anneal for Ni–P, vacuum bake for plated Ni). When possible, temperature slopes are normalized to the bare-fiber value from the same study; if unavailable, the closest baseline is reported. These conventions allow the comparison of S_T^{coat}, η_T, hysteresis, and drift across diverse process routes. Representative quantitative multipliers for different metals—approximately 1.5× for Ni, 2× for Cu, 2.5× for Zn, and 3× for Sn—are summarized later in Section 3 and Figures 2 and 3 [69].

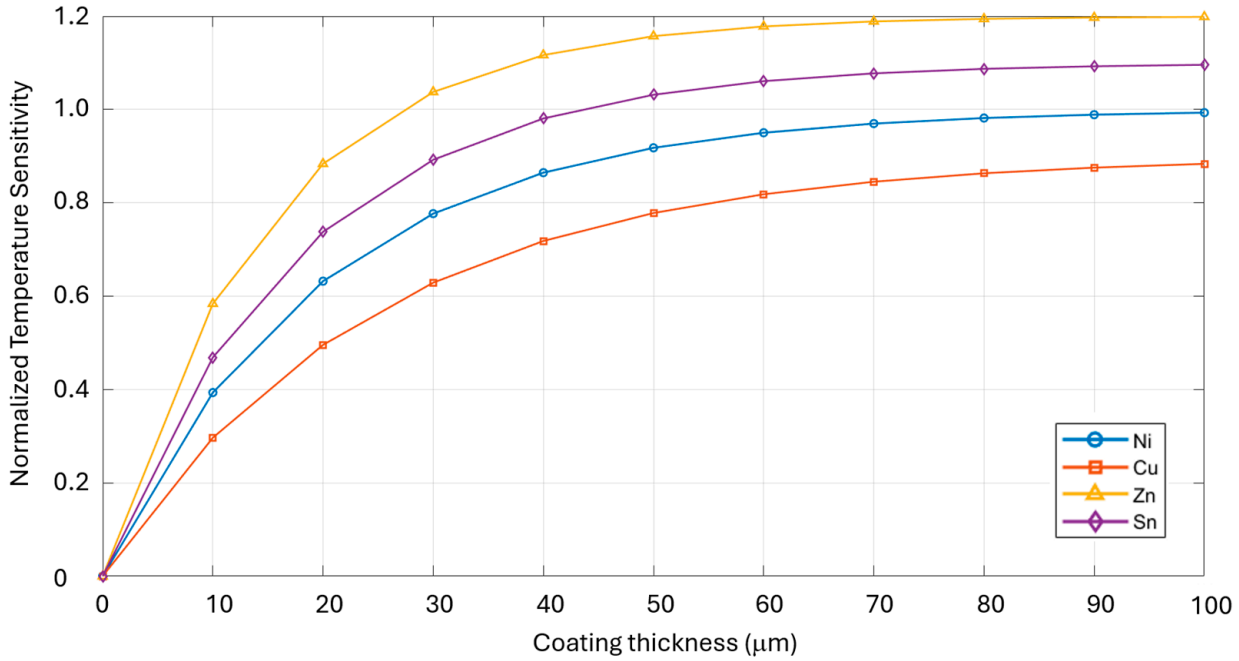

Figure 3. Normalized temperature sensitivity ($\eta_T = S_T^{coat}/S_T^{bare}$, see Section 2.3) as a function of coating thickness for Ni → Zn and Ni/Sn multilayers. The plateau trend denotes full thermo-mechanical coupling between the metal stack and the silica core. Representative behaviors are shown for Ni, Cu, Zn, and Sn coatings, based on trends reported in [27,38,42,63,67,68]. This figure illustrates the trade-off between coating thickness and diminishing returns in sensitivity gain. Data were consolidated from the indicated references and redrawn for clarity; curves represent representative trends rather than raw experimental data.

The described framework establishes how intrinsic FBG physics, thermo-mechanical coupling, and normalized sensitivity metrics are linked. These definitions underpin the comparative analysis of coating materials, deposition methods, and processing parameters presented in Sections 3–7, enabling the cross-study synthesis of temperature-sensitivity, stability, and durability trends [38,42,50,51,67–69].

3. Coating Materials and Design Constraints

The temperature response of a metalized FBG is governed by thermo-mechanical coupling between the coating and the silica fiber. As temperature changes, mismatch in CTE and differences in elastic modulus generate axial strain in the grating; the resulting

Bragg shift therefore depends on the coating's material, thickness, microstructure, and interface quality, in addition to the intrinsic thermo-optic and thermal-expansion terms of silica. Analytical and experimental studies consistently show a monotonic rise in sensitivity with thickness towards a plateau, after which additional build adds stress and defects with only marginal gain [38,42,67,68]. Design choices in this section are framed around reaching that plateau with the least residual stress and the highest spectral stability.

3.1. Material Families and Functional Roles

Metals are the primary workhorse because they combine high thermal conductivity, efficient strain transfer and robust attachment to glass. Nickel provides adhesion and a useful barrier/capping function; copper increases sensitivity and heat conduction but requires diffusion control at elevated temperatures; soft metals such as zinc, tin and indium excel at cryogenic temperatures thanks to larger CTE and lower modulus. In practice, duplex and multilayer stacks—e.g., Ni/Cu/Au or Ni → Zn—are adopted to balance adhesion, diffusion control and thermo-mechanical performance across wide temperature windows [27–31]. For deep-cryogenic operation, graded metallic stacks have demonstrated higher stability under cycling than single-layer counterparts while maintaining strong apparent slopes [29].

Polymeric overlayers (e.g., PMMA) can increase apparent sensitivity and ease cryogenic cycling but are limited by creep and upper-temperature stability [63,70]. Oxides and nitrides (TiN, TiO_2, ZnO) serve as chemically robust single layers or as thin barrier/cap layers that interrupt diffusion without imposing excessive stiffness; single-layer TiN deposited by ion-beam sputtering has shown clean, near-linear cryogenic behavior [54,55,59,61]. Functionally graded interlayers—such as Mo–Cu graded into an outer Ni coat—reduce residual stress and have demonstrated survival under thermal shock while maintaining useful slopes [46]. The broader literature on highly sensitive temperature-FBGs and nanostructured coatings reinforces these roles and clarifies the trade-offs between sensitivity and transient response [7,33].

3.2. Thickness Dependence and Optimal Ranges

Sensitivity increases with coating thickness until a material-dependent plateau is reached; beyond this knee, the gain per micrometer diminishes while residual stress, roughness and crack initiation risks grow [38,42,67]. EL Ni-P studies, for example, report slope growth from ≈12 to ≈19–20 pm/°C as thickness rises from ≈1 to ≈40 μm, followed by saturation; a short post-anneal removes λ(T) hysteresis (Section 3.4) [38,71]. PVD studies show clear thickness trends for Cu up to ≈0.76 μm [72], and thick sputtered Cu films can be pushed to tens of micrometers when protected by barriers/caps [64]. Duplex and multilayer stacks exploit material synergy to reach the plateau at lower individual-layer thicknesses, which reduces stress concentrations.

This plateau behavior is illustrated in Figure 3, which compares the sensitivity–thickness relationship for representative metallic coatings.

The data consolidated in Figure 3 highlight the nonlinear dependence of η^T on coating thickness, revealing two distinct regimes. At small thicknesses (<5 μm), partial strain transfer limits the apparent temperature sensitivity, and η^T increases nearly linearly with thickness. Beyond a critical or plateau value, η^T saturates, indicating full thermo-mechanical coupling between the coating and the silica substrate. This plateau typically occurs at 10–30 μm for Ni-based or Cu-based layers, and at smaller values for Zn and Sn coatings due to their lower elastic moduli and higher coefficients of thermal expansion. The saturation trend reflects a balance between increased thermo-elastic amplification and the onset

of residual stress, which can promote microcracking and spectral broadening if coating thickness continues to increase [27,38,42,63,67,68].

3.3. Cryogenic Behavior and Transients

At ≤80 K, soft-metal and Ni-based stacks typically raise apparent temperature sensitivity by ~1.5–5× relative to bare gratings, depending on metal and thickness [27,29,69]. This gain comes with a transient-response penalty: metallic overcoats increase thermal mass and often slow step response by about a factor of two under LN_2-type profiles, an effect highlighted in comparative thermal-sensing analyses [34,42]. Representative cryogenic sensitivity multipliers for Ni, Cu, Zn, and Sn coatings are illustrated in Figure 4, highlighting the enhanced apparent slopes relative to bare gratings (of apparent temperature sensitivity relative to bare FBGs are shown for Ni (~2× [27]), Cu (~2.5× [29]), Zn (~3.5× [69]), and Sn (~4× [57]) coatings). Reported behavior during cool-down can be mildly nonlinear, with some rate dependence; qualification should therefore include dynamic as well as quasi-static profiles [69]. Early high-field cryogenic tests also indicate that metal-coated FBGs maintain function under strong magnetic fields, which is relevant to fusion and accelerator environments.

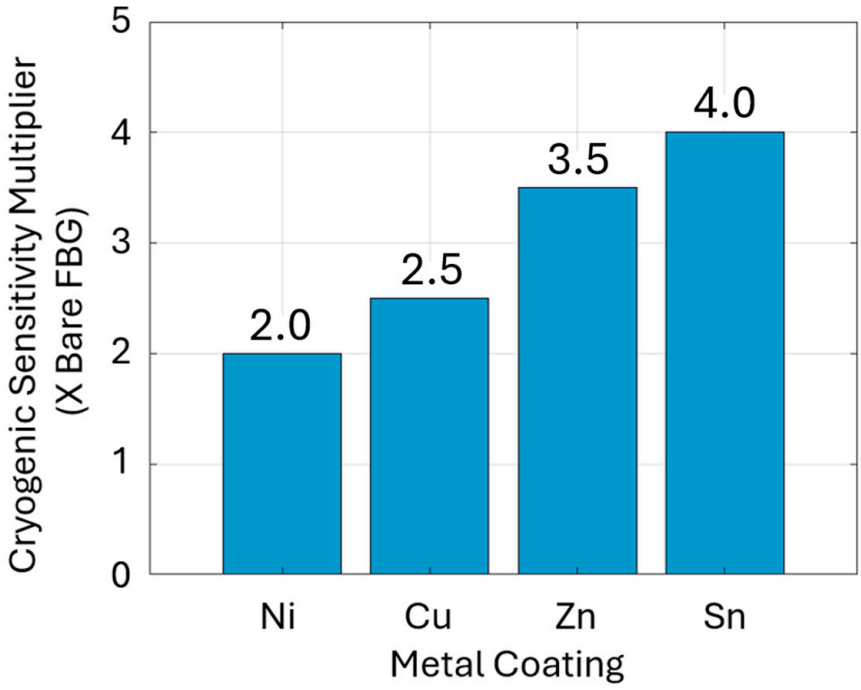

Figure 4. Representative enhancements of apparent temperature sensitivity relative to bare FBGs are shown for Ni (~2× [27]), Cu (~2.5× [29]), Zn (~3.5× [69]), and Sn (~4× [57]) coatings. The cryogenic sensitivity multiplier is equal to the bare FBG multiplied by a certain number. The trend reflects the larger coefficients of thermal expansion and lower modulus of soft metals at cryogenic temperatures. Literature-reported $+\eta^T$ multipliers for different coating materials and layer sequences. These are representative trends that have been redrawn for greater clarity and do not represent raw experimental data.

Figure 4 compares representative η^T multipliers obtained from different metallic coatings and multilayer stacks. The results emphasize the strong influence of both the metal's intrinsic thermal expansion and the stacking sequence on sensitivity enhancement. Zn- and Sn-based coatings provide the highest normalized sensitivities ($\eta^T \approx 2.5$–5) at cryogenic temperatures, whereas Ni- and Cu-based films yield smaller gains ($\eta^T \approx 1.2$–2) but superior mechanical and chemical stability. Multilayer and duplex designs, such as Ni

→ Zn or Ni/Sn, combine these effects, producing intermediate yet tunable responses. These observations confirm that the coating's thermo-mechanical properties and architecture can be tailored to achieve a desired balance between sensitivity amplification and robustness—a theme further analyzed in Sections 4–6.

3.4. Deposition Route, Microstructure, and Post-Treatments

The process route imprints microstructure and residual stress that strongly condition spectral stability. After $SnCl_2$ → $PdCl_2$ activation, EL Ni–P provides a conformal conductive seed at modest thermal budgets; it commonly exhibits λ(T) hysteresis that brief annealing (≈300 °C, ~60 min) removes [38,63]. Electroplated Ni builds thickness efficiently but absorbs hydrogen during deposition; a vacuum/thermal bake is required to stabilize the spectrum and avoid embrittlement [40]. PVD routes (sputtering, evaporation, ion-beam sputtering) deliver smooth seeds (Cr/Au, Ti) and functional films; ion-beam sputtered TiN shows stable, near-linear cryogenic slopes [59]. With suitable barriers/caps, sputtered Cu can be grown to substantial thickness and then cycled to high temperature and back to cryo [64]. CVD/ALD oxides (TiO_2, ZnO) offer conformal barriers and caps that reduce oxidation and interdiffusion at modest temperatures [54,55,61]. Hybrid schemes—PVD seed → electroplated Ni/Cu/Zn; regenerated gratings with Ti/Ag seed and Ni plating; or graded Mo–Cu → Ni stacks—combine adhesion, sensitivity and stress management, and show improved mid- to high-temperature performance with good model–experiment agreement at the lower end [31,46]. EL nanometal strategies and low-coarsening Ni-P metallization recipes broaden the wet-chemical toolkit specifically for fiber geometries [62,73]. Head-to-head comparisons across Ni, Cu, Zn and duplex stacks underline that process history governs the spread in reported gains as much as metallurgy itself [74].

3.5. Adhesion, Interfaces, and Seeding

Durable interfaces start with disciplined cleaning/etching and reliable seeding. The fiber-appropriate standard is $SnCl_2$ (sensitization) → $PdCl_2$ (activation) → EL Ni–P; Tollens' silvering and vacuum Cr/Au or Ti seeds are practical alternatives when chemistry or equipment dictates [45,48,49]. EL growth on silicate substrates is sensitive to pH, complexants and reducers; peel-test-oriented best practices on glass highlight the importance of bath housekeeping and staged deposition [50,75]. On a cylindrical dielectric, uniformity improves with rotation and gentle current-density ramps at plating start; staged builds preserve smooth interfaces and avoid stress concentrators [39,51].

3.6. High-Temperature Stability, Diffusion, and Barriers

At elevated temperature, Cu/Ni interdiffusion and oxidation dominate drift and mechanical degradation. Multilayer Ni/Cu/Au stacks maintain repeatable slopes to ~1000 °C under cycling when diffusion paths are interrupted and hydrogen introduced during plating is removed beforehand [30,42]. Duplex Cu/Ni stacks are prone to Kirkendall voiding above ~700–1010 °C unless buffered; barrier and cap layers, together with appropriate thermal budgets, mitigate this risk. Regenerated gratings with Ti–Ag–Ni stacks perform to ~600 °C with model–experiment agreement in the lower range [31]. Sputtered-Cu systems subjected to high-temperature treatment can retain integrity on return to cryo when barriers/caps are engineered correctly [64]. Figure 5 summarizes these comparative limits, contrasting the maximum stable operating temperature of single Ni and Cu coatings with that of Ni/Cu/Au multilayer stacks. Broader comparative evaluations concur that multilayer designs with explicit barriers and caps outperform single-metal coats as temperature rises [74].

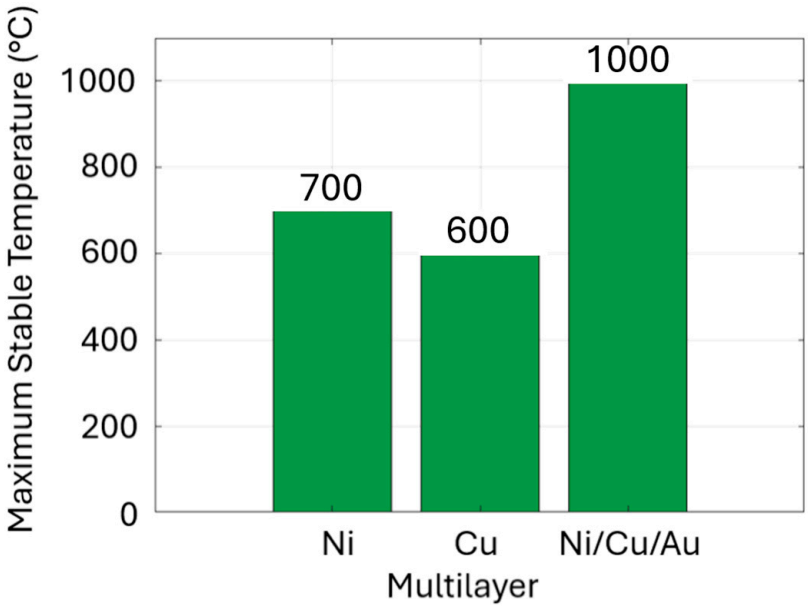

Figure 5. High-temperature stability of coated FBGs. Representative stability limits reported in the literature: single Ni coatings are stable up to ~700 °C before drift and embrittlement [30,40]; single Cu coatings degrade above ~600 °C unless capped [31]; Ni/Cu/Au multilayer stacks, with diffusion barriers, maintain integrity and repeatable slopes to ~1000 °C under cycling [64]. Data were consolidated from the indicated bibliographic references. These are representative trends that have been redrawn for greater clarity and do not represent raw experimental data.

3.7. Practical Selection Rules

Method selection should be driven by the target environment and the thickness–sensitivity plateau. For cryogenic service, soft metals or Ni-based duplexes (e.g., Ni → Zn) are favored for high apparent slopes; transient-response penalties should be anticipated and, where necessary, mitigated by thinner, higher-modulus caps or partially metalized geometries [27,29,34,41]. For high-temperature operation (≥600–1000 °C), multilayers with explicit barrier and cap layers (e.g., Ni/Cu/Au) are preferred to suppress diffusion and oxidation; hydrogen removal after plating is mandatory, and dwell at the highest temperatures should be limited or buffered [30,31,40]. Thickness should be allocated to reach the plateau without over-thickening any single constituent; modeling trends and Ni-P thickness studies provide practical guidance [38,42,67]. Interfaces should be engineered with proven seeds (Sn → Pd → EL Ni–P, or Ag/Cr–Au/Ti where appropriate), smooth transitions, staged builds and rotation for uniformity [39,45,48,49,51]. Here, diffusion control or stress relief is required; thin TiN/oxide caps, noble-metal barriers, or graded Mo–Cu interlayers are effective [46,54,59]. With these rules, stacks can be tailored to deliver the desired sensitivity while preserving spectral quality and durability across the intended temperature window.

4. Deposition Techniques

Coatings for FBGs are produced by a small set of process families whose physics shape adhesion, stress, microstructure, and, ultimately, spectral stability. For clarity, methods are grouped as top-down physical-vapor deposition (PVD), bottom-up CVD/ALD, wet-chemical routes (EL and ED), hybrid flows that combine these, and fusion-based approaches for direct integration into metals. This organization follows established thin-film taxonomies and usage across the optical-fiber literature and process primers [32–34,40].

4.1. Top-Down: PVD

PVD methods—magnetron sputtering, ion-beam sputtering and thermal/e-beam evaporation—provide dense, well-controlled films with good thickness uniformity along the fiber and around the grating region. They are widely used to create seeds that promote adhesion and conductivity before plating (e.g., Cr/Au or Ti), but they can also deliver functional single layers and multilayers in their own right [31,45]. Technique choice and parameters (pressure, power, gas, motion) govern intrinsic stress and microstructure; compressive stress from energetic bombardment improves density but can aggravate curvature-induced strain on cylindrical substrates if unmanaged. Single-layer TiN by ion-beam sputtering illustrates a PVD-only sensing coat, yielding a near-linear cryogenic slope of ≈10.7 pm/°C from 25 to −195 °C with strong chemical robustness [59]. Copper sputtering has been used as both a stand-alone sensing layer and a constituent of multilayers; thickness-dependent gains are reported up to ≈0.76 µm in simple studies [72], while thick magnetron Cu films (≈20 µm) have endured high-temperature treatments and subsequently operated down to 4.2 K when diffusion is actively managed by barrier or cap layers [43]. For high-temperature operation, multilayer Ni/Cu/Au stacks combine adhesion, conduction and diffusion control and have demonstrated repeatable slopes under cycling towards ~1000 °C when interfaces block interdiffusion pathways [30]. Cathodic-arc sources, though highly ionized, can eject macroparticles that seed roughness unless filtered or steered; magnetron and ion-beam sputtering therefore remain defaults for smooth films on fibers [60].

4.2. Bottom-Up: CVD and ALD

CVD and especially ALD are used to form conformal oxide caps and barriers at modest temperatures. Thin ZnO and TiO_2 on fiber geometries have shown stable thermal responses and illustrate the utility of conformal growth on curved substrates [54,55,61]. Growth rates are lower than in PVD and plating, but the conformality and stoichiometric control of CVD/ALD make them attractive for diffusion-barrier or oxidation-resistant over-layers above metallic stacks, or as adhesion-promoting primers when used thin enough to avoid excessive stiffness.

4.3. Wet-Chemical Routes: EL and ED

Wet-chemical methods dominate when thick, conformal metal builds are needed at low thermal budgets. A widely adopted workflow is $SnCl_2 \rightarrow PdCl_2$ activation on silica, deposition of an EL Ni–P seed, and ED of the target metal to the desired thickness. [48]. This route is attractive because the seed forms at a relatively low temperature and the subsequent ED step scales efficiently. Fiber-specific re-coating and metallization methods—including Tollens' silvering, tailored EL nanometal approaches, and Ni-P metallization without fiber coarsening—expand the toolbox and provide practical bath windows and housekeeping guidance for cylindrical dielectrics [52,62,64,76]. Two post-treatments are essential for spectral stability: a short anneal removes λ(T) hysteresis in Ni-P, and a vacuum/thermal bake after Ni ED outgasses hydrogen that would otherwise cause slow drift or embrittlement during cycling [38,41]. These wet-chemical routes underpin many cryo-oriented stacks. Comparative tests under dynamic cooling show metal coats raise the apparent cryogenic slope relative to bare gratings, with typical multipliers of ~1.5× (Ni), ~2× (Cu), ~2.5× (Zn) and ~3× (Sn), albeit with some rate-dependence during cool-down [69]. Ni → Zn combinations (EL Ni seed followed by Zn ED) and related zinc routes—derived from sputter-seeded or EL seeds—have been validated for low-temperature sensitivity and durability, with recipe control important to maintain λ_0 stability [29,57,58]. Where mechanical integration is desired, ED can be used to surface-mount FBGs directly onto

metallic substrates, achieving linear slopes (~30.7 pm/°C) and survival to high temperatures before the joint fails; in these cases, the interface—not the grating—becomes the limiting element [77]. As with any galvanic process on small cylinders, uniformity benefits from fiber rotation and gentle current-density ramps at the start of each run; staged EL builds with spectral quality assurance (QA) checkpoints prevent roughness and voiding that accumulate during long single immersions [39].

4.4. Hybrid and Combination Strategies

Combining PVD with plating, or mixing metals in duplex and multilayer stacks, allows sensitivity targets to be met while controlling diffusion and stress. A graded metal approach tailored for cryogenic service offers a complementary path to sensitivity and reliability without over-thick single layers [32]. Cross-study comparisons further confirm the duplex/multilayer advantage and highlight the importance of disciplined seeding and post-treatments [74]. A representative approach is a PVD seed (Ti or noble metal) followed by electroplated Ni, which provides adhesion and rapid thickness build; regenerated gratings with Ti/Ag seeds → Ni plating exemplifies improved mid- to high-temperature performance with model–experiment agreement at the lower end of the range [32]. Duplex Ni/Cu stacks are widely reported; an etchless Cu seed plus Ni plate improves slope and repeatability over Ni-only coatings in the 30–100 °C range [63], while Ni → Zn provides a robust cryogenic path with central-wavelength stability managed by recipe control [29,57]. For very high temperatures, Ni/Cu/Au multilayers use Ni as a barrier/base, Cu for conduction and sensitivity, and Au as a cap to limit oxidation and outward diffusion; careful interface control and post-plating hydrogen removal are prerequisites for stability towards ~1000 °C [30]. Residual-stress management improves further with functionally graded interlayers. A Mo–Cu gradient beneath an outer Ni coat reduces stress concentrations and has demonstrated survival under thermal shock up to ~800 °C with slopes around 15 pm/°C [46]. Such graded stacks are particularly valuable when embedding in metallic hosts or when repeated high-temperature cycles are expected. Beyond the coating stacks themselves, broader compilations of metallic-coating effects at cryogenic temperatures confirm the thickness sensitivity and transient trends summarized here and help prioritize metals for duplexes [53].

In Section 6, Table 5 summarizes the relative merits of these process families in terms of achievable thickness, conformality, growth rate, and process complexity. It serves as a compact technical data sheet for coated FBGs.

4.5. Fusion-Based Approaches and Integration into Metals

A complementary path is to integrate the grating directly into a metallic component. Casting experiments embedding FBGs in aluminum alloys have shown reproducible axial response and negligible hysteresis when the grating is appropriately prepared and positioned, confirming the feasibility of fusion-based integration for structural applications [78]. Thick-metal builds on long-period gratings illustrate the stress pitfalls of very heavy deposits and motivate staged growth and stress-relief steps for any fiber-based structure [47]. Looking forward, kinetic (cold) spray—a solid-state deposition process with high rates—offers a potential route to metal over-jackets or ex situ metallization of carriers that hold the FBG, though direct application to bare fibers demands careful control of particle impact to avoid damage [56].

5. Surface Preparation and Activation

Reliable coatings on silica fibers start with disciplined surface preparation. Residual polymer, drawing lubricants and handling films impede adhesion and must be removed be-

fore metallization. A typical sequence begins with solvent cleaning (acetone or isopropanol with brief ultrasonics), followed by a mild chemical etch to activate the silica surface; dilute mineral acids or alkalis are selected to suit the downstream chemistry, with thorough deionized rinsing between stages to prevent cross-contamination. Excessive etching increases flaw size and should be avoided on sensing sections. The aim is a clean, lightly roughened surface that promotes nucleation without compromising fiber strength. General thin-film practice notes on stress and roughness control complement these steps and are particularly relevant on cylindrical substrates [48,63]. Activation of the glass for EL deposition is most commonly achieved with $SnCl_2$ sensitization followed by $PdCl_2$ activation. Tin(II) species adsorb on silica and reduce palladium in situ, leaving catalytic Pd^0 sites that initiate autocatalytic growth in the EL bath. Rinses between $SnCl_2$ and $PdCl_2$ are critical; chloride carry-over into the Ni–P bath degrades deposit quality. Alternative seeds are useful when chemistry or equipment dictates the following: Tollens' silvering provides a rapid aqueous conductive layer that can be over-plated immediately, and vacuum-deposited Cr/Au or Ti seeds provide very smooth, adherent underlayers that are especially valuable when later ED is planned [45,48,49,73,74,76]. For fibers that will receive thick metal builds, a conformal EL Ni–P seed is widely used because it forms uniformly at modest temperature and pH, wets glass well after Sn/Pd activation, and produces a conductive, mechanically robust surface for subsequent ED. Operating near 90 °C and pH ≈ 4.5–5.0 yields continuous films with low porosity; bath aging and contamination are the usual causes of nodular growth and must be monitored. Thickness should be accumulated in stages, with spectral checks between stages, because single long immersions tend to raise internal stress and roughness; practical studies on fibers show that pushing a single EL step beyond a few tenths of a micrometer increases the risk of voiding and cracking [38,39,75]. EL Ni–P coatings also exhibit λ(T) hysteresis; short post-deposition annealing (≈300 °C for ~60 min, inert/vacuum) removes this effect and stabilizes the slope for subsequent cryogenic cycling [38]. Table 3 summarizes the main stages of this workflow, including representative parameters, quality checks, and references. It provides a structured overview of surface preparation and activation for coated FBGs.

Once a conformal seed is in place, ED supplies thickness efficiently for Ni, Cu, Zn, Sn and their combinations. Uniformity on a small cylinder is improved by rotating the fiber and by using gentle current-density ramps at the start of each run to control nucleation and minimize local heating. Chemistry dictates current density, additives and agitation; for example, tin baths are commonly operated at 0.4–0.6 A dm^{-2} to mitigate whisker formation without sacrificing rate, whereas Ni/Cu typically run at 1–5 A dm^{-2} depending on geometry and agitation [48]. Because the current distribution is naturally non-uniform around a dielectric cylinder, auxiliary electrodes and judicious anode–cathode spacing help regularize the field. Spectral quality should be verified after each plating increment before further build-up or metal changes are attempted. Table 4 summarizes representative bath chemistry, current densities, temperatures, and agitation practices for these metals. It serves as a quick reference for commonly used ED parameters in coated FBGs.

Two post-treatments are essential for spectral stability after wet metallization. EL Ni–P requires the brief anneal mentioned above to remove hysteresis; electroplated Ni (and, to a lesser extent, Cu) benefits from a vacuum or thermal bake to outgas hydrogen absorbed during deposition. Without this step, slow spectral drift and embrittlement can appear during subsequent cycling [41,73,78]. Where Cu/Ni stacks are used and high-temperature exposure is anticipated, barrier or cap layers should be included to suppress interdiffusion and oxidation, and the thermal budget of downstream processing should be planned accordingly [30,38]. For zinc-containing stacks intended for cryogenic service, recipe discipline is important to maintain central-wavelength stability across thermal

cycles [29,57]. Fiber-specific re-coating and metallization procedures provide additional, practical windows for activation, seeding and build without fiber coarsening [52,62,73,76].

Interface integrity is governed as much by process discipline as by materials choices. Cleanliness between steps, controlled rinsing and bath-renewal schedules reduce particulate defects and pinholes that would otherwise seed delamination. When PVD seeds are employed, magnetron or ion-beam sputtering is preferred for smooth films on fibers; unfiltered cathodic-arc sources eject macroparticles that can imprint roughness and stress concentrators unless they are filtered or steered appropriately [45,60]. Regardless of route, in-process spectral QA—tracking Bragg-centroid position, FWHM and SNR before coating, after activation/seed, after each thickness increment, and after any post-treatment—provides early warning of adhesion issues or stress build-up and allows recipes to be corrected before the final build is committed. When coatings are intended to operate in contact with hosts or joints, surface preparation must be coordinated with the packaging route. Electroplated surface-mounted joints can bond fibers directly onto metallic substrates and survive high temperatures before the joint fails; in such cases, the interface rather than the grating becomes the limiting element [77]. Foundational studies of apparent strain, temperature–strain discrimination and embedded configurations inform how to interpret the coated sensor's response when it is constrained by surrounding materials and how to compensate or calibrate for these effects [79–83]. Broader compilations of metallic-coating effects at cryogenic temperatures are consistent with the process-linked trends summarized here and help prioritize metals and thickness allocations for cryogenic builds [53].

6. Comparative Synthesis and Qualification

Comparative evaluation of coating routes shows that performance is determined as much by deposition method and process control as by material choice. Across EL, electroplated, sputtered, and hybrid stacks, reported gains vary widely, but converging patterns are clear [30,31,38,40,41,47,50,64,67,68,72]. Table 5 synthesizes these trends, comparing thickness range, conformality, growth rate, stress, and defect susceptibility for the main families. Wet-chemical approaches, including EL Ni–P and ED of Ni, Cu, Zn, or Sn, are efficient for building thickness at modest cost but require rigorous control of bath composition, additives, and current density to avoid hydrogen uptake, roughness, or coarsening [38,40,62].

Vacuum-based processes such as sputtering or ALD/CVD yield smoother, conformal films and effective barrier/cap layers. TiN, TiO_2, and ZnO grown by these methods show stable performance under both cryogenic and high-temperature cycling [54,55,59,61]. Hybrid approaches—PVD seed plus electroplated builds, regenerated gratings with Ti–Ag–Ni, or multilayer Ni/Cu/Au stacks—consistently extend stability and sensitivity by combining adhesion, diffusion control, and bulk builds [30,31,47,50,64]. Qualification focuses on reproducibility and stability under cycling. Metrics include slope repeatability, spectral drift, SNR, FWHM, and hysteresis, with thresholds reported across cryogenic, high-temperature, and radiation environments [27,29,34,41,44,69,80]. Table 6 consolidates tolerance ranges, while Figure 5 illustrates the comparative high-temperature stability of single Ni, single Cu, and Ni/Cu/Au multilayers, highlighting the importance of diffusion barriers and hydrogen removal [30,31,42,64]. A recurring limitation in the literature is inconsistent reporting of processing details such as activation, seeding, thickness allocation, and annealing. Without this information, cross-study comparisons remain qualitative. To address this gap, Table 7 proposes a per-specimen reporting template, aligned with best practices from related sensor domains [39,50,60,75]. Adoption of such standards would enable reproducibility, meta-analysis, and eventual benchmarking of coating performance across laboratories. In synthesis, the comparative evidence underscores that multilayer and hy-

brid stacks outperform single-metal coatings, but reliable qualification depends equally on adherence to standardized metrics and reporting practices. Establishing these frameworks is essential for advancing coated FBG technologies from experimental demonstrations to deployable sensing solutions.

The comparative data in Tables 2–5 demonstrate that coating design and deposition route exert a comparable influence on performance. EL–ED sequences typically deliver higher η^T at cryogenic conditions, whereas hybrid PVD-seeded routes offer better uniformity and stability at high temperature. These trends are consistent with the thermal and mechanical models introduced in Section 2, reinforcing the importance of tailoring both material selection and process architecture.

To consolidate the comparative discussion above, Table 8 summarizes the main coating families, their recommended application domains, and indicative accuracy ranges derived from the reviewed literature. It classifies the main coating families used for FBGs and summarizes their preferred application domains. Metallic and duplex coatings dominate cryogenic and moderate-temperature operation owing to their high strain-transfer efficiency, while ceramic and oxide films are preferred in high-temperature and oxidizing environments. Hybrid and composite coatings extend durability by combining mechanical and chemical protection. Reported normalized sensitivities (η^T) vary from ≈1 for polymeric layers up to ≈5 for optimized multilayers, corresponding to practical temperature accuracies between ±0.3 K and ±1 K depending on calibration and interrogation method. These comparisons provide a framework for selecting coating strategies according to environmental constraints and accuracy targets.

7. Design Recommendations and Outlook

The literature converges on a practical principle. The best coated-FBG design reaches the sensitivity plateau with minimal residual stress. It also suppresses diffusion and hydrogen effects that destabilize spectra. For deep-cryogenic service (≤80 K), duplex designs that pair a nickel base with a soft metal provide the clearest gains. Ni → Zn and Ni + Sn routes consistently deliver large apparent-slope multipliers over bare fibers, provided recipes are disciplined and central wavelength is stabilized across cycling [27,29,57,69]. The EL Ni–P seed (after $SnCl_2 \rightarrow PdCl_2$) should be grown in staged dips, briefly annealed to remove λ(T) hysteresis, and then over-plated; any electroplated Ni requires a vacuum/thermal bake to outgas hydrogen [38,40]. Cryogenic gains come with a transient penalty. Metal buildup increases thermal mass, which can slow steps by about two times in representative systems. Therefore, fast-transient applications may favor thinner, higher-modulus caps or partially metalized geometries to recover response time [34,41]. When maximizing cryogenic slope under aggressive cycling, graded metallic architectures are a practical alternative to very thick single-metal layers [32]. Between 80 and 300 K, the emphasis shifts to balance. Duplex Ni/Cu stacks combine nickel's adhesion and barrier role with copper's higher thermal conductivity and expansion, meeting sensitivity targets at moderate total thickness. Where fast transients dominate or chemical robustness is paramount, thin TiN (PVD) single layers offer clean, near-linear cryogenic behavior with minimal mass penalty [59]. Diffusion control should be planned even if nominal operation is below 573.15–673.15 K (300–400 °C); thin barriers or caps (e.g., TiN/oxides or Au) keep Cu/Ni interactions in check as temperature excursions increase [30,54,55,61]. For high-temperature regimes (600–1000 °C), failure modes are set by interdiffusion and oxidation. Ni/Cu/Au multilayers—Ni as base/barrier, Cu for conduction/sensitivity, Au as oxidation-resistant cap—are the most reliable pattern in the literature, achieving repeatable slopes under cycling towards ~1273.15 K (1000 °C) when diffusion paths are interrupted and when any hydrogen from wet metallization is removed beforehand [30,40]. Regenerated gratings with Ti/Ag seeds and plated Ni

perform into the mid-temperature range with model–experiment agreement at the lower end [31]. Where thermal-shock or embedding is expected, functionally graded Mo–Cu → Ni interlayers reduce residual-stress concentrations while maintaining useful slopes [46]; surface-mounted electroplated joints are viable for direct bonding to metal substrates, with the joint often becoming the limiting element rather than the grating [77]. When gratings are embedded or constrained by hosts, interpretation of the apparent temperature slope should follow composite-beam logic rooted in foundational apparent-strain and discrimination studies [47,56,78,79]. Two cross-cutting choices dominate outcomes across all windows. First, thickness allocation: once the sensitivity–thickness curve approaches its knee, further metal is better spent on stress management or barriers/caps than on chasing marginal slope increases [38,42,67]. Second, process history: seeding, staged growth, and post-treatments determine microstructure and residual stress and therefore spectral stability. Benchmark comparisons emphasize that reported gains align when recipes, seeds and post-treatments are standardized across studies [74]. Fiber-specific metallization methods (re-coating procedures, EL nanometal strategies, fiber-safe Ni–P recipes) and general thin-film practice notes are what make these designs reproducible across labs [35,48,52,62,73,76]. Field overviews and cryogenic FBG surveys ensure the recommendations sit within the wider sensing landscape and application demands in aeronautics, energy and fusion [5–7,10,23–25]. Looking forward, three directions are poised to have the biggest payoff. Response-time optimization at low temperature—via thinner, higher-modulus caps, improved thermal pathways to the host, or partial metallization—can capture sensitivity gain while recovering temporal performance. Diffusion-aware design at the hot end—explicit barrier selections, noble caps, and dwell-time limits for Cu/Ni interfaces—extends stability towards the top of the range. And integration pathways that treat coatings and packaging together—graded interlayers for embedded mounts, electroplated surface joints—shrink the gap between laboratory coupons and deployable assemblies [46,77,78]. A disciplined reporting template and acceptance bands will further improve comparability and accelerate recipe transfer between groups [2,3]. A standardized reporting format is needed to improve cross-laboratory reproducibility. Table 7 provides an example of a log template for each specimen that captures essential details from surface preparation through qualification. This enables direct comparison of results across different coating routes and laboratories.

8. Conclusions and Outlook

A coherent picture emerges from the survey. Apparent temperature sensitivity in coated FBGs increases with metal thickness and then saturates, so the most effective designs reach a plateau with minimum residual stress and with diffusion and hydrogen effects actively managed. In practice, this means distributing thickness across duplex or multilayer stacks, engineering interfaces deliberately ($SnCl_2$ → $PdCl_2$ activation; EL Ni–P seed; smooth PVD seeds where needed), and applying post-treatments—short annealing for EL Ni–P and vacuum/thermal baking after ED—that erase process memory before qualification. For deep cryogenic work, Ni combined with soft metals (Ni → Zn or Ni + Sn) yields the largest slope multipliers, at the expense of a slower step response; recipe discipline is required to stabilize central wavelengths across cycles. Between 80 and 300 K, duplex Ni/Cu provides a balanced sensitivity–transient trade-off; thin TiN offers a fast-response and PVD-only alternative with clean cryogenic behavior. At high temperature (600–1000 °C), failure modes are diffusion and oxidation; Ni/Cu/Au multilayers with explicit Ni barriers and noble caps enable repeatable slopes under cycling toward ~1000 °C, provided that the hydrogen introduced during wet metallization is removed beforehand. When joining to or embedding in metals, graded Mo–Cu → Ni interlayers control residual stress, and electroplated surface-mounted joints shift the limiting element from the grating to the interface. Evi-

dence syntheses focused on cryogenic-coated FBGs and on thermal-sensing performance analyses corroborate the thickness–sensitivity and transient trends highlighted here. These technical conclusions sit within a broader sensing context captured by field surveys and overviews of optical-fiber sensors and networks. Application exemplars in aeronautics and energy—including aeronautical SHM, conceptual cryogenic/energy systems and fusion divertor monitoring—underscore the operational constraints that coatings help address. Foundational studies on apparent strain and temperature–strain discrimination remain central when interpreting coated FBGs in constrained or embedded configurations. General thin-film/process primers and fiber-specific metallization playbooks (re-coating procedures, EL nanometal strategies, fiber-safe Ni–P recipes) help transfer recipes between laboratories and explain why apparently similar stacks can diverge without process discipline. A recent cryogenic-FBG review further justifies the emphasis on coatings in low-temperature regimes. The case for graded cryogenic stacks and the superiority of duplex/multilayer strategies at elevated temperature is supported by both focused demonstrations and broad comparative evaluations. Overall, hybrid route planning—PVD or EN seeding, electroplated builds, thin barriers/caps, and graded interlayers where needed—sits near the Pareto front across cryogenic, ambient, and high-temperature windows. Standardizing acceptance bands and adopting per-specimen logs will accelerate comparability and deployment. The most promising near-term opportunities are (i) response-time optimization at low temperature without surrendering sensitivity; (ii) diffusion-aware designs at the hot end, with explicit dwell-time management for Cu/Ni interfaces; and (iii) integration-first stacks that treat coatings and packaging as a single design object.

Recommendations for Coating Selection and Future Development

Based on the comparative analysis presented, the coating selection for FBGs should primarily consider the operational environment and sensitivity required. Metallic coatings (Ni, Cu, Al) are recommended for cryogenic and moderate-temperature sensing due to their excellent strain-transfer efficiency, while duplex and multilayer systems (Ni $\rightarrow$ Zn, Ni/Sn, Ni/Cu/Au) offer tunable thermal response and improved adhesion for broader temperature spans. Ceramic and oxide coatings (Al_2O_3, SiO_2, TiO_2) remain the best option for long-term, high-temperature, oxidizing environments, whereas hybrid or composite stacks provide mechanical robustness and corrosion protection for embedded or structural applications.

Future development should focus on scalable, precisely controlled deposition techniques such as electrodeposition, ALD, and hybrid PVD/ED approaches to ensure uniformity and reproducibility on optical fibers. Nanoscale interlayers and diffusion barriers are essential for stress management and adhesion under thermal cycling. In parallel, integration with additive manufacturing and laser-assisted microdeposition could enable localized reinforcement and multifunctional coatings. Combining these approaches with data-driven optimization of process parameters can accelerate the transition toward next-generation industrial FBG sensors with high reliability and adaptability for aerospace, energy, and cryogenic applications.

Author Contributions: Conceptualization, C.V. and M.A.C.; methodology, R.D.; validation, C.V. and M.A.C.; investigation, E.D.M.; formal analysis C.V. and E.D.M.; resources, E.D.M. and C.V.; data curation, E.D.M. and R.D.; writing—original draft preparation, C.V. and E.D.M.; writing—review and editing, C.V., R.D. and M.A.C.; visualization, E.D.M.; supervision, C.V.; project administration, C.V. and M.A.C.; funding acquisition, C.V. All authors have read and agreed to the published version of the manuscript.

Funding: This work was supported by the CREATION (CRyogenic Efficiency gAins Through optImized nanO-structured metal coatiNgs, B83C25000880005) research project.

Acknowledgments: The authors gratefully acknowledge the members of the CREATION consortium for constructive discussions and for sharing technical insights that helped refine the coating route classifications, stack archetypes, and qualification criteria consolidated in this review.

Conflicts of Interest: The authors declare no conflicts of interest. The funders had no role in the design of the study; in the collection, analyses, or interpretation of data; in the writing of the manuscript; or in the decision to publish the results.

Abbreviations

The following abbreviations are used in this manuscript:

ALD	Atomic Layer Deposition
CTE	Coefficient of Thermal Expansion
CVD	Chemical Vapor Deposition
ED	Electrodeposition
EL	Electroless
FBG	Fiber Bragg Grating
FWHM	Full-Width at Half Maximum
IBS	Ion Beam Sputtering
ML	Multilayer
PMMA	Poly(Methyl MethAcrylate)
PVD	Physical Vapor Deposition
QA	Quality Assurance
SNR	Signal-to-Noise Ratio

References

1. Lo Presti, D.; Massaroni, C.; D'Abbraccio, J.; Saccomandi, P.; Caponero, M.A.; Polimadei, A.; Schena, E. Fiber Bragg Gratings for Medical Applications and Future Challenges: A Review. *IEEE Access* **2020**, *8*, 156863–156888. [CrossRef]
2. Xie, J.F.; Zhang, H.; Zhu, Z.; Xu, J.N.; Hu, R.H.; Song, L.F. A Study of the Temperature Sensitivity of Fiber Bragg Gratings after Metallization. *Smart Mater. Struct.* **2007**, *16*, 1837–1842. [CrossRef]
3. Lupi, C.; Montinaro, N.; Paolozzi, A.; Giordano, M.; Russo, S.; Mastrogiacomo, F.; Campopiano, S.; Cutolo, A.; Cusano, A. Critical Issues of Double-Metal Layer Coating on FBG for Applications at High Temperatures. *Sensors* **2019**, *19*, 3824. [CrossRef]
4. Liu, Y.; Fang, J.; Jia, D.; Li, W. Temperature Characteristics of FBG Sensors with Different Coatings for High Temperature Superconductor Application. In Proceedings of the 2019 IEEE 3rd International Electrical and Energy Conference (CIEEC 2019), Beijing, China, 7–9 September 2019; Institute of Electrical and Electronics Engineers (IEEE): Piscataway, NJ, USA, 2019; pp. 1546–1550. [CrossRef]
5. Pendão, C.; Silva, I. Optical Fiber Sensors and Sensing Networks: Overview of the Main Principles and Applications. *Sensors* **2022**, *22*, 7554. [CrossRef]
6. Vendittozzi, C.; Felli, F.; Lupi, C. Modeling FBG Sensors Sensitivity from Cryogenic Temperatures to Room Temperature as a Function of Metal Coating Thickness. *Opt. Fiber Technol.* **2018**, *42*, 84–91. [CrossRef]
7. Mishra, V.; Lohar, M.; Amphawan, A. Improvement in Temperature Sensitivity of FBG by Coating of Different Materials. *Optik* **2016**, *127*, 825–828. [CrossRef]
8. Wang, X.D.; Wolfbeis, O.S. Fiber-Optic Chemical Sensors and Biosensors (2015–2019). *Anal. Chem.* **2020**, *92*, 397–428. [CrossRef] [PubMed]
9. Ramakrishnan, M.; Rajan, G.; Semenova, Y.; Farrell, G. Overview of Fiber Optic Sensor Technologies for Strain/Temperature Sensing Applications in Composite Materials. *Sensors* **2016**, *16*, 99. [CrossRef] [PubMed]
10. Wen, C.; Li, Y. Effects of Metal Coating on the Fiber Bragg Grating Temperature Sensing Characteristics. *J. Mod. Opt.* **2016**, *63*, 762–770. [CrossRef]
11. Campanella, C.E.; Cuccovillo, A.; Campanella, C.; Yurt, A.; Passaro, V.M.N. Fibre Bragg Grating Based Strain Sensors: Review of Technology and Applications. *Sensors* **2018**, *18*, 3115. [CrossRef]

12. Wang, X.; Wang, W.; Li, Q.; Xie, C.; Luo, G.N. Application of FBG sensors in tokamak tungsten divertor, component for strain and temperature monitoring. In *Optics and Photonics for Energy and the Environment*; ET5A.6. 10.1364/EE.2018.ET5A.6; Optica Publishing Group: Washington, DC, USA, 2018.
13. Hegde, G.; Asokan, S.; Hegde, G. Fiber Bragg grating sensors for aerospace applications: A review. *ISSS J. Micro Smart Syst.* **2022**, *11*, 257–275. [CrossRef]
14. Yassin, M.H.; Farhat, M.H.; Soleimanpour, R.; Nahas, M. Fiber Bragg grating (FBG)-based sensors: A review of technology and recent applications in structural health monitoring (SHM) of civil engineering structures. *Discov. Civ. Eng.* **2024**, *1*, 151. [CrossRef]
15. Lupi, C.; Vendittozzi, C.; Ciro, E.; Felli, F. FBG Spectrum Regeneration by Ni-Coating and High-Temperature Treatment. *Sensors* **2022**, *22*, 7255. [CrossRef]
16. Nogueira, R.; Oliveira, R.; Bilro, L.; Heidarialamdarloo, J. New advances in polymer fiber Bragg gratings. *Opt. Laser Technol.* **2015**, *78*, 104–109. [CrossRef]
17. Mihailov, S.J.; Grobnic, D.; Hnatovsky, C.; Walker, R.B.; Lu, P.; Coulas, D.; Ding, H. Extreme Environment Sensing Using Femtosecond Laser-Inscribed Fiber Bragg Gratings. *Sensors* **2017**, *17*, 2909. [CrossRef]
18. Leal-Junior, A.; Frizera, A.; Marques, C. Development and Characterization of UV-Resin Coated Fiber Bragg Gratings. *Sensors* **2020**, *20*, 3026. [CrossRef] [PubMed]
19. Wang, X.; Sun, X.; Hu, Y.; Zeng, L.; Liu, Q.; Duan, J. Highly-Sensitive Fiber Bragg Grating Temperature Sensors with Metallic Coatings. *Optik* **2022**, *262*, 169337. [CrossRef]
20. Deng, Y.; Jiang, J. Optical Fiber Sensors in Extreme Temperature and Radiation Environments: A Review. *IEEE Sens. J.* **2022**, *22*, 11145–11161. [CrossRef]
21. Stephen, J.; Pal, P.; Mathew, J. Advances in Cryogenic Temperature Sensing Using Fiber Bragg Grating: A Review. *IEEE Sens. J.* **2025**, *25*, 12345–12360. [CrossRef]
22. Zaynetdinov, M.; See, E.M.; Geist, B.; Ciovati, G.; Robinson, H.D.; Kochergin, V. A Fiber Bragg Grating Temperature Sensor for 2–400 K. *IEEE Sens. J.* **2015**, *15*, 1908–1912. [CrossRef]
23. Hisham, H. *Fiber Bragg Grating Sensors: Development and Applications*; Taylor & Francis Group, LLC: Boca Raton, FL, USA, 2019; ISBN 978-0-367-22485-1. [CrossRef]
24. Ciotti, M.; Nardelli, V.; Caponero, M.A.; Felli, F.; Lupi, C.; Ippoliti, L. An Optical System for Cryogenic Temperature Measurements. *Smart Mater. Struct.* **2007**, *16*, 1708–1711. [CrossRef]
25. Soman, A.C.; Chalackal, A.T.; Kanakambaran, S. Design of Cryogenic Temperature Sensors Using Copper-Coated Fiber Bragg Gratings. In Proceedings of the 2022 IEEE Region 10 Symposium (TENSYMP 2022), Kolkata, India, 29–31 May 2022; Institute of Electrical and Electronics Engineers (IEEE): Piscataway, NJ, USA, 2022. [CrossRef]
26. Chiuchiolo, A.; Bracco, C.; Rossi, F.; Bianchi, L.; Verdi, M. Cryogenic Test Facility Instrumentation with Fiber Optic and Fiber Optic Sensors for Testing Superconducting Accelerator Magnets. In *IOP Conference Series: Materials Science and Engineering*; Institute of Physics Publishing: Bristol, UK, 2017; Volume 278, p. 012082. [CrossRef]
27. Feng, Y.; Zhang, H.; Li, Y.L.; Rao, C.F. Temperature Sensing of Metal-Coated Fiber Bragg Grating. *IEEE/ASME Trans. Mechatron.* **2010**, *15*, 511–519. [CrossRef]
28. Sugino, M.; Ogata, M.; Mizuno, K.; Hasegawa, H. Development of Zinc Coating Methods on Fiber Bragg Grating Temperature Sensors. *IEEE Trans. Appl. Supercond.* **2016**, *26*, 9000606. [CrossRef]
29. Wang, X.; Sun, X.; Hu, Y.; Duan, J. Multilayer Metal-Coated Fiber Bragg Grating for High-Temperature Sensing. *Measurement* **2024**, *226*, 114132. [CrossRef]
30. Shiue, S.T.; Yang, C.H.; Chu, R.S.; Yang, T.J. Effect of the Coating Thickness and Roughness on the Mechanical Strength and Thermally Induced Stress Voids in Nickel-Coated Optical Fibers Prepared by Electroless Plating Method. *Thin Solid Films* **2005**, *485*, 169–175. [CrossRef]
31. Butt, M.A. Thin-Film Coating Methods: A Successful Marriage of High-Quality and Cost-Effectiveness—A Brief Exploration. *Coatings* **2022**, *12*, 1115. [CrossRef]
32. Muench, F. Electroless Plating of Metal Nanomaterials. *ChemElectroChem* **2021**, *8*, 3591–3600. [CrossRef]
33. Barhoum, A.; García-Betancourt, M.L.; Jeevanandam, J.; Hussien, E.A.; Mekkawy, S.A.; Mostafa, M.; Omran, M.M.; Abdalla, M.S.; Bechelany, M. Review on Natural, Incidental, Bioinspired, and Engineered Nanomaterials: History, Definitions, Classifications, Synthesis, Properties, Market, Toxicities, Risks, and Regulations. *Nanomaterials* **2022**, *12*, 177. [CrossRef] [PubMed]
34. Elsherif, M.; Salih, A.E.; Muñoz, M.G.; Alam, F.; AlQattan, B.; Savariraj, A.D.; Zaki, M.F.; Yetisen, A.K.; Park, S.; Wilkinson, T.D.; et al. Optical Fiber Sensors: Working Principle, Applications, and Limitations. *Adv. Photonics Res.* **2022**, *3*, 2100371. [CrossRef]

35. Grandal, T.; Piñeiro, E.; Asensio, A.; Rodriguez, F. Metallic Coating Techniques for Fiber Bragg Grating Sensors. In Proceedings of the 8th Iberoamerican Optics Meeting and 11th Latin American Meeting on Optics, Lasers, and Applications, Porto, Portugal, 22–26 July 2013; SPIE: Bellingham, WA, USA, 2013; p. 878538. [CrossRef]
36. Majumder, M.; Gangopadhyay, T.K.; Chakraborty, A.K.; Dasgupta, K.; Bhattacharya, D.K. Fibre Bragg Gratings in Structural Health Monitoring—Present Status and Applications. *Sens. Actuators A* **2008**, *147*, 150–164. [CrossRef]
37. Kern, W.; Schuegraf, K.K. Deposition Technologies and Applications: Introduction and Overview. In *Handbook of Thin Film Deposition Processes and Techniques*, 1st ed.; Noyes Publications: Park Ridge, NJ, USA, 1988; pp. 1–44.
38. Rao, C.; Zhang, H.; Feng, Y.; Xiao, L.; Ye, Z. Thick Metal Coating Long-Period Fiber Grating. In Proceedings of the 6th International Symposium on Advanced Optical Manufacturing and Testing Technologies: Design, Manufacturing, and Testing of Smart Structures, Micro- and Nano-Optical Devices, and Systems, Xiamen, China, 26–29 April 2012; SPIE: Bellingham, WA, USA, 2012; p. 84181Q. [CrossRef]
39. Koo, K.N.; Lee, J.H.; Kim, S.H.; Park, J.; Lee, S.H. Fabrication and Modification of Temperature FBG Sensor: Role of Optical Fiber Type and Cu Sputtered Thickness. *Phys. Scr.* **2020**, *95*, 095602. [CrossRef]
40. Tang, A.Q.; Fang, L.; Xue, S.J.; Yin, B.; Liu, L.; Zhang, P. Ni-P Coating Metallization on Fiber Bragg Grating without Fiber Coarsening and Its Temperature Sensing Property. In Proceedings of the 2011 International Conference on Optical Instruments and Technology: Optical Sensors and Applications, Beijing, China, 6–9 November 2011; SPIE: Bellingham, WA, USA, 2011; p. 819907. [CrossRef]
41. Zhao, Z.B.; Gillispie, B.A.; Smith, J.R. Coating Deposition by the Kinetic Spray Process. *Surf. Coat. Technol.* **2006**, *200*, 4746–4754. [CrossRef]
42. Scurti, F.; McGarrahan, J.; Schwartz, J. Effects of Metallic Coatings on the Thermal Sensitivity of Optical Fiber Sensors at Cryogenic Temperatures. *Opt. Mater. Express* **2017**, *7*, 1754–1764. [CrossRef]
43. Li, Y.; Yang, K.; Li, X. Temperature Sensing Characteristics of Metal Coated FBG during Dynamic Cooling Process. *Opt. Fiber Technol.* **2018**, *45*, 368–375. [CrossRef]
44. Sengupta, D.; Sai Shankar, M.; Saidi Reddy, P.; Sai Prasad, R.L.N.; Narayana, K.S.; Kishore, P. An Improved Low-Temperature Sensing Using PMMA Coated FBG. In *Optics InfoBase Conference Papers, Proceedings of the Asia Communications and Photonics Conference and Exhibition 2011, Shanghai China, 13–16 November 2011*; SPIE: Bellingham, WA, USA, 2011. [CrossRef]
45. Jin, L.; Zhang, W.; Zhang, H.; Liu, B.; Zhao, J.; Tu, Q.; Kai, G.; Dong, X. An embedded FBG sensor for simultaneous measurement of stress and temperature. *IEEE Photonics Technol. Lett.* **2006**, *18*, 154–156. [CrossRef]
46. Mattox, D.M. Arc Vapor Deposition. In *Handbook of Physical Vapor Deposition (PVD) Processing*; Elsevier: Amsterdam, The Netherlands, 2010; pp. 287–300. [CrossRef]
47. Pawar, K.; Dixit, P. A critical review of copper electroless deposition on glass substrates for microsystems packaging applications. *Surf. Eng.* **2022**, *38*, 576–617. [CrossRef]
48. Prasad, R.D.; Teli, B.; Prasad, R.S.; Prasad, R.B.; Prasad, S.R.; Sinha, P.; Sinha, A.; Sinha, P.; Saxena, M.; Prasad, R.R.; et al. A Review on Thin Film Technology and Nanomaterial Characterization Techniques. *ES Mater. Manuf.* **2024**, *25*, 1198. [CrossRef]
49. Li, C.; Liu, M.; Song, H.; Wang, J.; Wu, Y.; Chen, X. Thermal Sensing Performance Analysis, Preparation and Application of Bimetallic Layer MFBG. *Int. J. Heat Mass Transf.* **2023**, *215*, 124514. [CrossRef]
50. Listewnik, P. Temperature Fiber-Optic Sensor with ZnO ALD Coating. *Eng. Proc.* **2021**, *2*, 99. [CrossRef]
51. Zhang, P.; Wang, X.; Guan, M.; Xin, C.; Wu, W.; Lin, X.; Pei, B. Enhanced Strain and Temperature Sensing in Copper-Coated Fiber Bragg Grating Sensors across a Wide Temperature Range from Cryogenic to Elevated Levels. *Cryogenics* **2024**, *139*, 103834. [CrossRef]
52. Perry, M.; Niewczas, P.; Johnston, M.; Mackersie, J. Nickel plating of FBG strain sensors for nuclear applications. In Proceedings of the 21st International Conference on Optical Fiber Sensors, Ottawa, ON, Canada, 15–19 May 2011; Bock, W.J., Albert, J., Bao, X., Eds.; SPIE: Bellingham, WA, USA, 2011; Volume 7753. Article 77530C. [CrossRef]
53. Shen, R.-S.; Teng, R.; Li, X.-P.; Zhang, J.; Xia, D.-C.; Fan, Z.-Q.; Yu, Y.-S.; Zhang, Y.-S.; Du, G.-T. Electroless Nickel Plating and Electrodeposition on FBG Temperature Sensor. *Chem. Res. Chin. Univ.* **2008**, *24*, 635–639. [CrossRef]
54. Wang, Y.L.; Tu, Y.; Tu, S.T. Development of Highly-Sensitive and Reliable Fiber Bragg Grating Temperature Sensors with Gradient Metallic Coatings for Cryogenic Temperature Applications. *IEEE Sens. J.* **2021**, *21*, 4652–4663. [CrossRef]
55. Li, Y.; Wen, C.; Zhang, H.; Yang, J.; Yan, M.; Jiang, J. An Electrodeposition Method for Surface Mounting Optical Fiber Sensors on the Metal Substrate. *IEEE Photonics Technol. Lett.* **2016**, *28*, 1811–1814. [CrossRef]
56. Tu, Y.; Qi, Y.H.; Tu, S.T. Fabrication and thermal characteristics of multilayer metal-coated regenerated grating sensors for high-temperature sensing. *Smart Mater. Struct.* **2013**, *22*, 075026. [CrossRef]

57. Li, Y.; Hua, Z.; Yan, F.; Gang, P. Metal coating of fiber Bragg grating and the temperature sensing character after metallization. *Opt. Fiber Technol.* **2009**, *15*, 391–397. [CrossRef]
58. Mansor, N.F.; Raja Ibrahim, R.K. Temperature sensitivity of FBG coating with zinc oxide and silicon carbide. *J. Phys. Conf. Ser.* **2021**, *1892*, 012033. [CrossRef]
59. Kesavan, K.; Ravisankar, K.; Senthil, R.; Sundaram, B.A.; Parivallal, S. Studies on Apparent Strain Using FBG Strain Sensors for Different Structural Materials. *Exp. Tech.* **2014**, *38*, 31–38. [CrossRef]
60. Lindner, M.; Gaßmann, S.; Klein, T.; Roeser, F.; Möllmann, M.; Lerch, R. Fiber Bragg Sensors Embedded in Cast Aluminum Parts: Axial Strain and Temperature Response. *Sensors* **2021**, *21*, 1680. [CrossRef] [PubMed]
61. Freitas, R.; Araujo, F.; Araujo, J.; Neumann, H.; Ramalingam, R. A Study on Intermediate Buffer Layer of Coated Fiber Bragg Grating Cryogenic Temperature Sensors. In *IOP Conference Series: Materials Science and Engineering*; Institute of Physics Publishing: Bristol, UK, 2015; Volume 101, p. 012154. [CrossRef]
62. He, J.; Ding, L.; Cai, J.; Zhu, W.; Dai, J. A Novel High Temperature Resistant Mo-Cu Functional Gradient Coating for Optic Fiber Bragg Grating. *Results Phys.* **2019**, *14*, 102456. [CrossRef]
63. Weraneck, K.; Lee, S.W.; King, N.; Ward, A.D.; Haynes, M.; Sampson, P.; Allwood, D. Strain Measurement in Aluminium Alloy during the Solidification Process Using Embedded Fibre Bragg Gratings. *Sensors* **2016**, *16*, 1853. [CrossRef] [PubMed]
64. Li, Y.; Wang, Y.; Wen, C. Temperature and Strain Sensing Properties of the Zinc Coated FBG. *Optik* **2016**, *127*, 6463–6469. [CrossRef]
65. Kok, S.P.; Go, Y.I.; Wang, X.; Wong, M.D. Advances in Fiber Bragg Grating (FBG) Sensing: A Review of Conventional and New Approaches and Novel Sensing Materials in Harsh and Emerging Industrial Sensing. *IEEE Sens. J.* **2024**, *24*, 29485–29505. [CrossRef]
66. Hokkanen, A.; Salmi, A.; Vashistha, V.; Nyman, M.; Nielsen, S.K.; Jensen, T.; Jessen, M.; Wälchli, B.; Kapulainen, M.; Naulin, V.; et al. A Panda fiber temperature sensor up to 900°C. *J. Instrum.* **2022**, *17*, P07031. [CrossRef]
67. Lupi, C.; Felli, F.; Brotzu, A.; Caponero, M.A.; Paolozzi, A. Improving FBG Sensor Sensitivity at Cryogenic Temperature by Metal Coating. *IEEE Sens. J.* **2008**, *8*, 1299–1304. [CrossRef]
68. Listewnik, P.; Hirsch, M.; Struk, P.; Weber, M.; Bechelany, M.; Jędrzejewska-Szczerska, M. Preparation and Characterization of Microsphere ZnO ALD Coating Dedicated for the Fiber-Optic Refractive Index Sensor. *Nanomaterials* **2019**, *9*, 306. [CrossRef]
69. Sandlin, S.; Kinnunen, T.; Rämö, J.; Sillanpää, M. A Simple Method for Metal Re-Coating of Optical Fibre Bragg Gratings. *Surf. Coat. Technol.* **2006**, *201*, 3061–3065. [CrossRef]
70. Silva, D.; da Silva, L.F.; de Souza, R.F.; de Almeida, D.L.; de Oliveira, M.M. Sputtering Deposition of TiO_2 Thin Film Coatings for Fiber Optic Sensors. *Photonics* **2022**, *9*, 342. [CrossRef]
71. Lou, H.H.; Huang, Y. Electrodeposition. In *Encyclopedia of Chemical Processing*; Lee, S., Ed.; Taylor & Francis: New York, NY, USA, 2006.
72. Chan, T.H.T.; Seah, L.K.; Leung, A.Y.T.; Li, H.-N.; Lam, H.F. Fiber Bragg Grating Sensors for Structural Health Monitoring of Tsing Ma Bridge: Background and Experimental Observation. *Eng. Struct.* **2006**, *28*, 648–659. [CrossRef]
73. Hsu, C.Y.; Chiang, C.C.; Hsieh, T.S.; Hsu, H.C.; Tsai, L.; Hou, C.H. Study of Fiber Bragg Gratings with TiN-Coated for Cryogenic Temperature Measurement. *Opt. Laser Technol.* **2021**, *136*, 106768. [CrossRef]
74. Feng, Y.; Zhang, H.; Li, Y.-L.; Peng, G. Highly Sensitive Ni-Cu Duplex Metal Coated Fiber Bragg Grating Temperature Sensor. In Proceedings of the 2009 Symposium on Photonics and Optoelectronics, Wuhan, China, 14–16 August 2009; pp. 1–4. [CrossRef]
75. Li, Y.; Zhang, H.; Feng, Y.; Peng, G. A Plating Method for Metal Coating of Fiber Bragg Grating. *Chin. Opt. Lett.* **2009**, *7*, 115–117. [CrossRef]
76. Kok, S.; Go, Y.; Wang, X.; Wong, D. A Review of Nanostructure Coating Techniques to Achieve High-Precision Optical Fiber Sensing Applications. *Nanomanufacturing* **2024**, *4*, 214–240. [CrossRef]
77. Wright, R.F.; Buric, M.; Egbu, J.; Ziomek-Moroz, M.; Lu, P.; Ohodnicki, P.R. Electrolessly Coated Optical Fibers for Distributed Corrosion Monitoring. In Proceedings of the CORROSION 2019, Nashville, TN, USA, 24–28 March 2019; pp. 1–12. [CrossRef]
78. Rajini-Kumar, R.; Suesser, M.; Narayankhedkar, K.G.; Krieg, G.; Atrey, M.D. Performance Evaluation of Metal-Coated Fiber Bragg Grating Sensors for Sensing Cryogenic Temperature. *Cryogenics* **2008**, *48*, 142–147. [CrossRef]
79. Chanet, N.; Frigione, D.; Imbeaux, F.; Debieu, J.; Jacquet, P.; Mazon, D. Design and Integration of Femtosecond Fiber Bragg Gratings Temperature Probes inside Actively Cooled IT-ER-Like Plasma-Facing Components. *Fusion Eng. Des.* **2021**, *166*, 112376. [CrossRef]
80. Sala, G.; Di Landro, L.; Airoldi, A.; Bettini, P. Fibre Optics Health Monitoring for Aeronautical Applications. *Meccanica* **2015**, *50*, 2547–2567. [CrossRef]
81. Caloud, J.; Imbeaux, F.; Frigione, D.; Boulbe, C.; Jacquet, P.; Mazon, D. Conceptual Design of Fiber Bragg Grating Temperature Sensors for Heat Load Measurements in COMPASS-U Plasma-Facing Components. *Fusion Eng. Des.* **2023**, *193*, 113608. [CrossRef]

82. Wang, X.; Zhang, Y.; Li, H.; Li, S.; Huang, Y.; Liu, Y. R&D of a Strain Monitoring System for the EAST Tungsten Divertor. *Nucl. Mater. Energy* **2019**, *19*, 498–502. [CrossRef]
83. Chang, T.; Jia, L.; Sui, Q.; Cui, H.-L. High-Temperature Measurement Using Cu-Plating Fiber Bragg Grating for Metal Smart Structure Applications. In *Sensors and Smart Structures Technologies for Civil, Mechanical, and Aerospace Systems 2014*; SPIE: Bellingham, WA, USA, 2014; p. 90613P. [CrossRef]